10.1515/astro-2017-0149

Baltic Astronomy, vol. 22, 77–99, 2013

PECULIARITIES AND VARIATIONS IN THE OPTICAL SPECTRUM OF THE RV TAURI-TYPE STAR R SCT

Tõnu Kipper[1] and Valentina G. Klochkova[2]

[1] *Tartu Observatory, Tõravere, 61602, Estonia; tk@aai.ee*

[2] *Special Astrophysical Observatory RAS, Nizhnij Arkhyz, 369167, Russia; valenta@sao.ru*

Received: 2013 March 15; accepted 2013 April 17

Abstract. We analyzed some new high resolution optical spectra of the semiregular RV Tauri-type star R Sct. Fundamental parameters were found to be $T_{\rm eff} = 4500$ K, $\log g = 0.0$ and $\xi_{\rm t} = 4.0$ km s^{-1}. The results of chemical analysis show that R Sct is a metal-poor star with [Fe/H]≈ -0.5. The carbon content with respect to iron is significantly larger than in the Sun, [C/Fe] = 0.84, but there is an evident deficiency of heavy elements. We found no tight correlation of the chemical abundances on the condensation temperatures of elements. This means that in R Sct the depletion by condensation into dust does not work, with possible exception of Ca and Sc. The luminosity derived from the Hipparcos parallax corresponds to a tip of the red-giant branch or slightly above it. Thus it is possible that R Sct evolved off the early-AGB when it has not yet experienced the third dredge-up in thermal pulses, or it is still located on AGB. The peculiarities of spectral features (emissions, line-splitting) and the complicated time-variable radial velocities were also studied.

Key words: stars: atmospheres – stars: individual: R Sct

1. INTRODUCTION

The RV Tauri-type stars are luminous ($4 > \log(L/L_\odot) > 3.2$) pulsating variables located in the Hertzsprung-Russell diagram between the cepheids and the long-period variables. Their masses are quite low $0.8 > M/M_\odot > 0.5$, and the periods of luminosity changes are between 30 to 150 days (Wallerstein & Cox 1984). Their light curves show large irregularities both in period and shape of semiperiodic variations with alternation of deep and shallow minima. There are two photometric classes of light curves of RV Tauri-type stars. The RVa class contains stars with constant mean magnitude, and the RVb class variables show the variation of the mean magnitude on a time-scale of about 600 to 1500 d. Many RV Tauri stars exhibit two dominant periods: variations with short period ($P \approx 40$ d) of small amplitude are superimposed on variations of equal or larger amplitude with longer period ($P \approx 800$ d) (Giridhar et al. 1994). Spectroscopically, Preston et al. (1963) by low-resolution spectra divided them into classes A, B and C. The group A consists of stars of spectral classes G and K. The group B consists of Fp(R) stars with very peculiar spectra. The spectra of group C stars are similar to B but without strong bands of molecules containing carbon. They also exhibit strong hydrogen emission lines during light maxima.

RV Tauri stars are located at the top of the Population II instability strip and are generally considered to be post-AGB stars (Jura 1986). Their masses anticipated from the pulsational analysis are $M = 0.3 - -0.7\,M_{\odot}$ (Fokin 1994). However, RV Tauri stars do not exhibit the expected for the post-AGB stage high abundances of carbon and s-process elements. They often show abundances similar to the depletion patterns in the gas phase of interstellar medium (ISM). The dust-induced depletion is possible as RV Tauri stars are thought to be mostly binaries with the dust possibly confined in a disk (Ruyter et al. 2005).

Matsuura et al. (2002) argue that the brightest member of the class, R Sct, may be still a thermally-pulsing AGB star, observed in a helium-burning phase.

This work is devoted to spectroscopy of this most irregular variable among the RV Tauri stars, which has a period close to 142 d. Photometrically R Sct is a RVa star and spectroscopically it belongs to Preston's group A. The basic parameters of R Sct, as listed in the SIMBAD database, are presented in Table 1.

The parallax given in Table 1 has been obtained with Hipparcos (Van Leeuwen 2007). If the period-luminosity relation of cepheids is used, the distance should be as large as 750 pc, which corresponds to luminosity of 9400 $L_{\odot}$ (Ruyter et al. 2005). The spectral type of R Sct is strongly variable: from G0 Iae to K2p(M3) Ibe. Wing (1987) has found that in 1985 spectral type of R Sct was similar to M5.3.

2. SPECTRAL OBSERVATIONS AND REDUCTIONS

For the investigation we used two high resolution spectra ($R = 45\,000$) of R Sct obtained on 2010 July 30 and September 24 with the Nasmyth Echelle Spectrograph (Panchuk et al. 2009), which is permanently located at the Nasmyth focus of the 6 m telescope of the Special Astrophysical Observatory.

Table 1. Basic parameters of R Sct = HD 173819 (SIMBAD database).

Coordinates	α (2000)	18 47 28.95
	δ (2000)	–05 42 18.54
Galactic coordinates	ℓ	27.4031°
	b	–01.7218°
Mean magnitude	B	6.70
	V	5.41
Spectral type		K0 Ibpv
Parallax π (mas)		2.32 ± 0.82
Distance d (pc)		431

The spectrograph was equipped with an image slicer (Panchuk et al. 2009). A CCD camera with 2048 × 2048 pixels (15×15 μm, readout noise $7e^{-}$) produced by the Copenhagen University Observatory was used as a detector. The spectra cover the wavelength region 442–593 nm (JD = 2455408.5) and 522–669 nm (JD = 2455464.3).

We have also used two spectra taken from the NARVAL database[1]. NARVAL is a new generation stellar spectropolarimeter copied from the ESPaDOnS on the CFHT and adapted to the 2 m telescope Bernard Lyot atop of Pic du Midi (Donati 2007)[2]. The spectra were observed on 2007 September 5 and 2008 June 4. They cover the wavelength region 360–1048 nm, have the resolution of about $R = 65\,000$ and the signal-to-noise ratio from 10 at short wavelengths to about 250 in the red.

The brightness of the star during the observations was close to the mean value. The two NARVAL spectra were obtained at $V \approx 5.1$, at the local maximum of the

[1] http://tblegacy.bagn.obs-mip.fr/narval.html)

[2] Donati J.-F. 2007, http://tblegacy.bagn.obs-mip.fr/projects/narval/v1/press1-eng.html

light curve and at $V \approx 5.7$ on the rising part of the light curve. The SAO spectra were obtained at $V \approx 5.7$ on the horizontal part of the light curve and $V \approx 5.4$ on the declining light.

The spectra were reduced using the NOAO astronomical data analysis facility IRAF. The use of image slicer results in three parallel strips of spectra in each order, shifted in wavelengths. Therefore all strips were reduced separately, linearized in wavelengths and coadded. We checked the accuracy of this procedure (Kipper & Klochkova 2005) and found that the wavelengths of the terrestrial lines in the star spectrum are reproduced within a few 0.001 Å.

3. ANALYSIS

3.1. Atmospheric parameters

For the abundance determinations only the spectra obtained at SAO were used. As starting parameters we accepted the data found by Luck (1981): $T_{\rm eff} = 4400$ K, $\log g = 0.0$ and [Fe/H] = –0.9. The Kurucz model atmospheres for metal-deficient stars were applied[3]. By forcing the excitation equilibrium for the most numerous line set of Fe I (230 lines), we have found $T_{\rm eff} = 4500$ K. With this procedure also the microturbulent velocity $\xi_{\rm t} = 4.0 \pm 0.3$ km s^{-1} was fixed (see Figures 1 and 2).

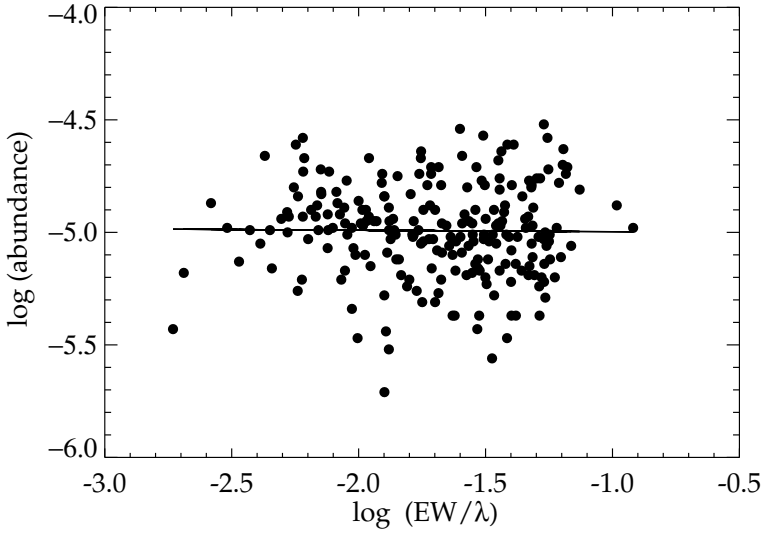

Fig. 1. Dependence of the iron abundance on Fe I line strengths. The plot is made for a microturbulent velocity of 4.0 km s^{-1}.

With this microturbulent velocity the iron abundance from Fe I lines is $\log \varepsilon$(Fe) = 7.00± 0.21. The number of useful Fe II lines is much smaller, and the determination of the microturbulent velocity is less accurate. Using quite numerous lines of Ni I we found $\xi_{\rm t} = 4.3$ km s^{-1}. The comparison of this value was used to estimate the error of $\xi_{\rm t}$ stated above. With the same $\xi_{\rm t} = 4.0$ km s^{-1} the iron abundance from Fe II lines is $\log \varepsilon$(Fe) = 7.15 ± 0.26. This shows that the assumed surface

[3] http://www.arm.ac.uk./csj/ccp7/Atlas/models/am05k2.dat and am10k2.dat

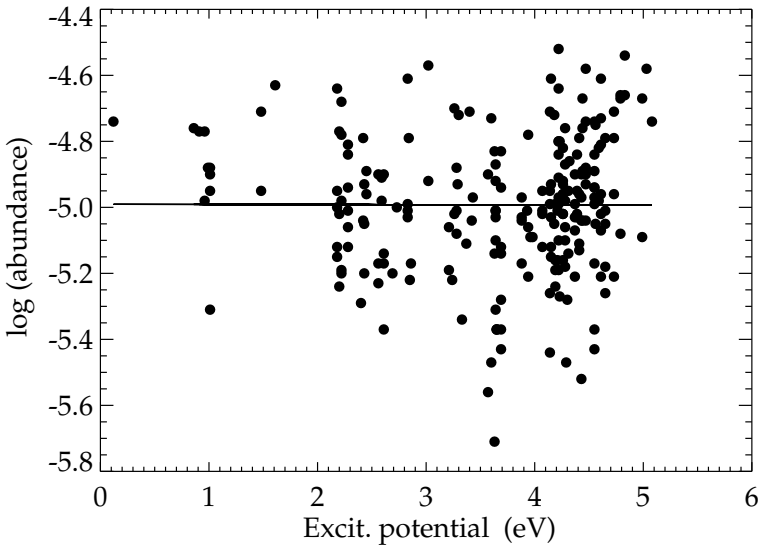

Fig. 2. Dependence of the iron abundance on Fe I line lower excitation potential. The plot corresponds to a microturbulent velocity of 4.0 km s^{-1} and $T_{\rm eff}$ = 4500 K.

gravity $\log g = 0.0$ is nearly correct with the error ≤ 0.2. If we accept a larger value of $\xi_{\rm t} = 4.7$ km s^{-1}, which seems to fit the Fe II lines better, then the abundances of Fe I and Fe II coincide.

These data are close to the earlier results of Giridhar et al. (2000), who found $T_{\rm eff}$ = 4500 K, $\log g = 0.0$, $\xi_{\rm t} = 3.0$ km s^{-1} and [Fe/H] = –0.4. R Sct was also studied earlier using low resolution spectra during the efforts to construct the spectral libraries for population synthesis (Prugniel et al. 2011; Cenarro et al. 2007). The results are comparable to our high resolution study.

The NARVAL spectra show definite split of lines already found by Preston (1962). The Fe I lines in these spectra correspond to somewhat higher temperature of about $T_{\rm eff}$ = 4750 K and a lower microturbulent velocity of 2 km s^{-1}. The iron abundance remains the same.

3.2. Abundances

The abundances of elements were derived with the help of the Kurucz program WIDTH5 or by spectral synthesis, when the hyperfine structure of lines was important, as for Mn I. Then the HFS data were taken from Kurucz's database[4]. For quite strong Mg I lines, the line damping was also taken into account, with the van der Waals damping constants from the same Kurucz line list, with an enhancement factor of 2.5.

The sources of oscillator strengths are indicated in Table 2, where the results on abundances are listed. The measured equivalent widths of lines, the used oscillator strength values and the derived abundances are listed in Table 4. Most of the oscillator strengths were taken from the NIST Atomic Spectra Database (Ralchenko et al. 2011) and from the SpectroWeb database (Lobel 2010).

[4] http://Kurucz.harvard.edu/linelists.html

Table 2. Chemical composition of R Sct. The number of the used lines and the sources of oscillator strengths are indicated in Notes.

El.	Sun[1]	R Sct		Remarks
	$\log\varepsilon$	$\log\varepsilon$	[El/H]	
H	12.00			
C	8.43	8.80 ± 0.24	0.37	4 C I, Sp.Web[2]
O	8.69	8.68 ± 0.05	0.02	2 O I, Sp.Web
Na	6.24	5.77 ± 0.07	–0.47	3 Na I, Sp.Web
Mg	7.60	7.51 ± 0.16	–0.09	5 Mg I, NIST[3]
Si	7.51	7.26 ± 0.12	–0.25	9 Si I, NIST
Ca	6.34	5.29 ± 0.19	–1.05	19 Ca I, NIST
Sc	3.15	1.64 ± 0.18	–1.51	6 Sc II, NIST, 2 Sc I, NIST
Ti	4.95	4.27 ± 0.25	–0.68	58 Ti I, NIST, 14 Ti II, Sp.Web
V	3.93	3.25 ± 0.19	–0.68	28 V I, NIST, 2 VII, Sp.Web
Cr	5.64	4.96 ± 0.22	–0.68	29 Cr I, NIST, 9 Cr II, Sp.Web
Mn	5.43	4.82 ± 0.34	–0.61	20 Mn I, Sp.Web
Fe	7.50	7.03 ± 0.22	–0.47	230 Fe I, 29 Fe II, NIST, Sp.Web
Co	4.99	4.40 ± 0.15	–0.59	24 Co I, Sp.Web, NIST
Ni	6.22	5.63 ± 0.18	–0.59	68 Ni I, NIST
Cu	4.19	3.38 ± 0.21	–0.81	2 Cu I, NIST
Zn	4.56	4.17 ± 0.10	–0.39	3 Zn I, Sp.Web
Y	2.21	0.24 ± 0.29	–2.45	4 Y II, NIST, Sp.Web
Ce	1.58	-0.24 ± 0.09	–1.82	2 Ce II, Sp.Web
Zr	2.58	1.24 ± 0.19	–1.34	7 Zr I, NIST
Ba	2.18	0.49 ± 0.10	–1.69	3 Ba II, Sp.Web
Nd	1.42	-0.11 ± 0.20	–1.52	7 Nd II, Har[4]
Sm	0.96	-0.58 ± 0.19	–1.54	3 Sm II, Sp.Web
Eu	0.52	-0.22	–0.74	1 Eu II, Sp.Web,Law[5]

[1] Asplund et al. (2009), relative to $\log\varepsilon$(H);
[2] SpectroWeb database, Lobel (2010);
[3] NIST Atomic Spectra Database, Ralchenko et al. (2011);
[4] Den Hartog et al. (2003);
[5] Lawler et al. (2001).

The results show that R Sct is a metal-poor star with $[\mathrm{Fe/H}] \approx -0.5$. Heavy elements are considerably underabundant. The same applies to Sc and Ca. A relatively high abundance of Eu is based on a single line. The carbon abundance is somewhat enhanced. If compared to the older solar abundance of 8.55 (Grevesse et al. 1996) this increase stays inside the error bar. This is an indication that the star could have experienced the third dredge-up on AGB. This event is expected to be accompanied by increase of s-process element abundances. Because this is not observed, the star cannot be in the post third dredge-up stage descending from the thermally pulsating AGB stars (Matsuura et al. 2002). However, there is a possibility of depletion of heavy refractory elements by the selective accretion from the dusty surroundings of the star. Recent abundance investigations of field RV Tauri stars (Rao & Reddy 2005) have revealed that stars with the intrinsic metallicity $[\mathrm{Fe/H}] > -1.0$, indicated by their S and Zn abundances, show an abnormal abun-

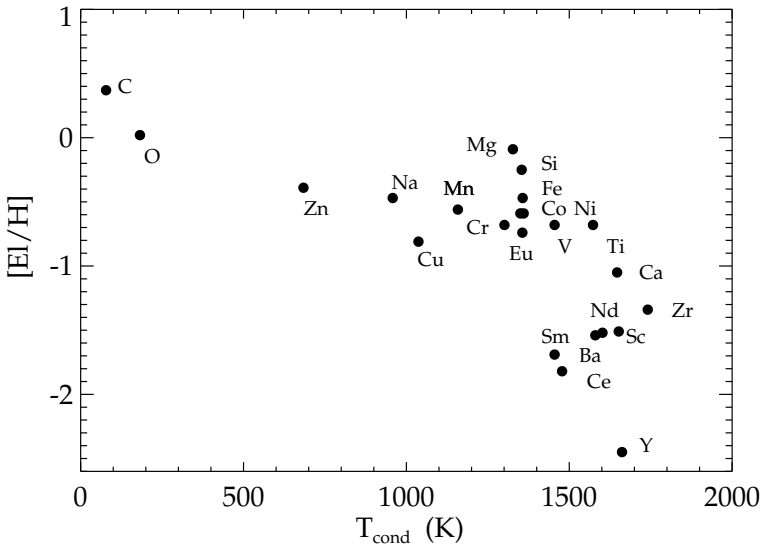

Fig. 3. Abundances of elements [El/H] for R Sct versus the corresponding condensation temperatures (Lodders 2003).

dance pattern. The elements with the condensation temperature $T_{\rm cond} > 1300$ K are selectively depleted.

In Figure 3 the abundances in R Sct are plotted against the condensation temperature of elements (Lodders 2003). As in other RV Tauri stars, we expect here a tight correlation of abundance anomalies with $T_{\rm cond}$. However, in the 1000–1600 K interval such dependence is not observed. Also there is an abrupt drop of abundances by 1 dex for $T_{\rm cond} > 1400$ K. In the overlapping temperature region the scatter is quite large. This means that in R Sct the depletion by selective condensation into dust and the subsequent accretion of refractory elements does not work. The conclusion about inefficiency of selective condensation is confirmed also by the Zn and Fe abundances: as follows from Table 2, [Zn/Fe] is close to the solar value. In this respect we confirm the results of Giridhar et al. (2000).

Rao & Reddy (2005) have analyzed the surface composition of cool RV Tauri star CE Vir and also found a deficiency of heavy elements. They also did not find any systematic trend in element depletions with the condensation temperature. Instead, a significant correlation of element deficiency with the first ionization potential (FIP) was discovered. This is an inverse effect in comparison with the abundance enhancement of elements with low FIP in the low speed solar wind and in the high speed streams.

In Figure 4 we have plotted abundances of elements [El/H] versus the first ionization potential (FIP) in R Sct. The abundances of elements with FIP < 7 eV are evidently reduced. But the dispersion of points is very large indicating that FIP effect is not the probable reason of underabundances of s-process elements.

Luck & Bond (1989) tried to explain underabundances of heavy elements in several RV Tauri stars by overionization of these elements by Lyman-continuum photons from a shock-wave passage. In Figure 5 we have plotted the abundances in R Sct versus the second ionization potential (SIP). The elements with

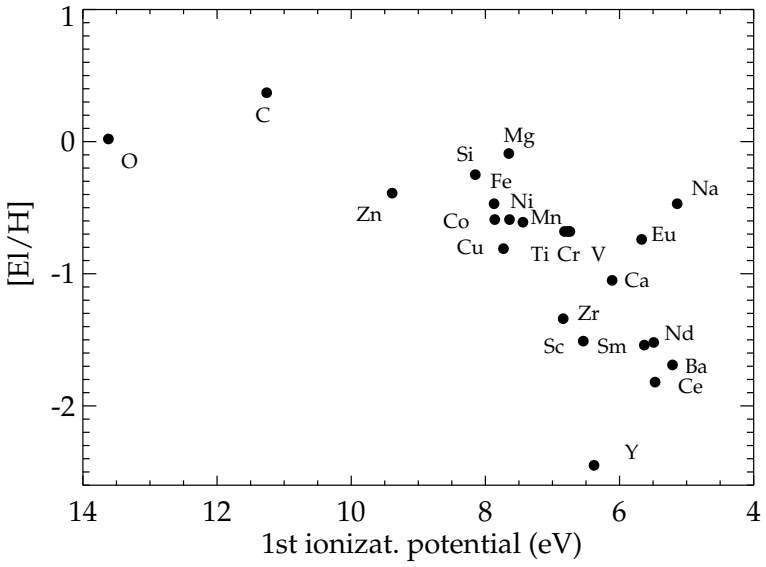

Fig. 4. Abundances [El/H] vs. the first ionization potential for R Sct.

SIP < 13.5 eV are clearly underabundant. The SIP of Na is very high, 47.3 eV, and the corresponding point (47.3,–0.47) is outside of figure limits. A relatively high abundance of Eu is very uncertain because it was derived from a single line. This dependence of underabundances on SIP does not allow to decide whether they are related to the third dredge-up on AGB.

4. SPECTRAL PECULIARITIES

4.1. Emission lines

High variability of the spectrum of R Sct during its pulsating periods was described earlier by Preston (1962) and Pollard et al. (1997). As the light of the star changes, most details in the spectrum also change significantly: emission and absorption components in the Hα profile, emissions in weak metallic lines of low excitation (Ti I) and a split of strong absorptions. Our R Sct spectra demonstrate the variability of all these spectral features.

The Balmer line changes in the spectrum of R Sct with the light variability has been studied in detail by Lebre & Gillet (1991a). In the SAO spectra, obtained on the horizontal part of light curve near the maximum and at the start of light decline, Balmer lines are in absorption (Figure 6). In this figure, the velocity for Hα is reduced by –15.8 km s^{-1}, a difference of solar velocities between different dates of observation.

The lines are completely different in the NARVAL spectra obtained during the rising part of light curve (Figure 7). At that time the mean radial velocity determined from metallic lines was 36.5 km s^{-1}.

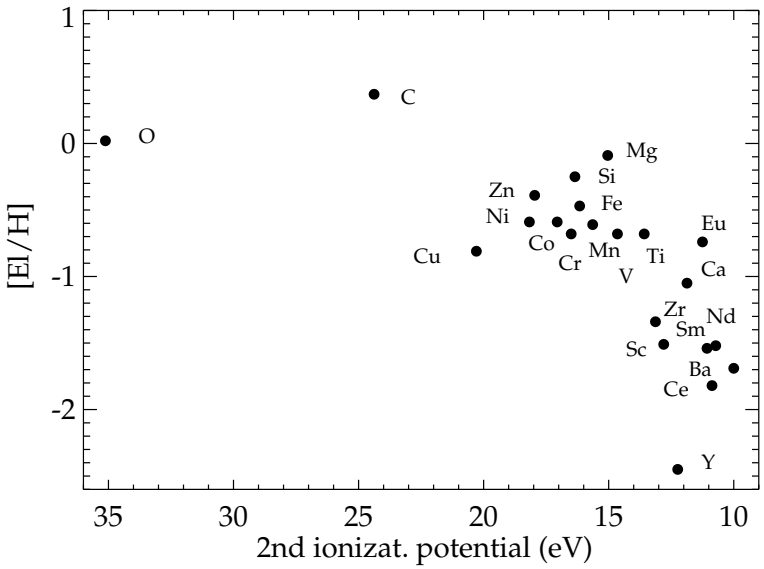

Fig. 5. Abundances [El/H] vs. the second ionization potential for R Sct.

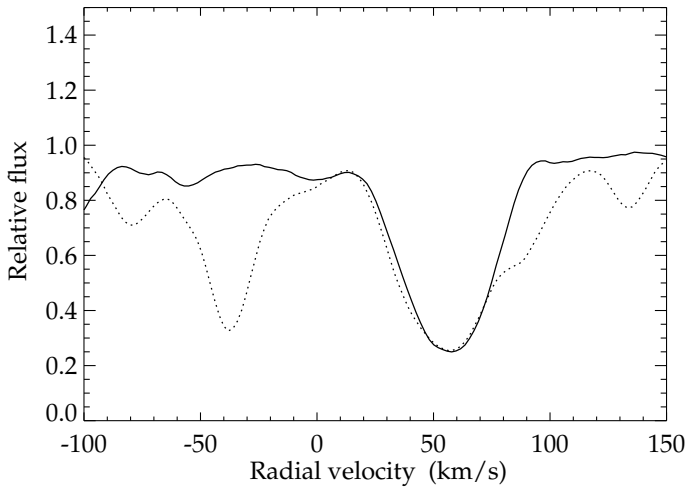

Fig. 6. The Hα (solid line) and Hβ (dotted line) lines in the spectrum of R Sct obtained at SAO on JD = 2455464.3 and JD = 2455408.5.

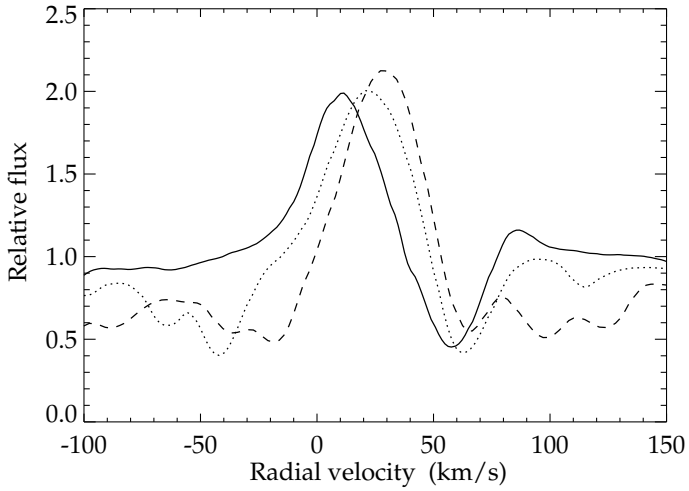

Fig. 7. The Hα (solid line), Hβ (dotted line) and Hγ (dashed line) lines in the spectrum of R Sct from the NARVAL database obtained on JD = 2454621.6.

The complicated profiles of weak metallic lines of low excitation (Fe I, Ti I, etc.) are known to exist in the R Sct spectrum during deep light minima (Howell et al. 1983). In the SAO spectrum obtained close to the light decline (JD = 2455464.3), numerous emission lines of Fe I and Ti I were identified. On the basis of 12 of the most reliable emissions, we obtained the average value of the radial velocity 42.6 ± 0.3 km s^{-1}. This means that the heliocentric velocity is close to 43.8 km s^{-1} found by Preston (1962).

In the NARVAL spectrum we also identified 58 emission lines originating from the low excitation levels (0.86–2.27 eV) of Ti I, V I and Fe I. The mean heliocentric velocity of these lines is 43.0 ± 1.5 km s^{-1}. Also, a Sc I line at 6305.65 Å with the velocity 45.2 km s^{-1} was found. These lines in the NIR spectral region show the clear P Cygni profiles (Figure 8).

Mozurkewich et al. (1987) found that the velocity of metallic emissions is variable with a half amplitude of about 4 km s^{-1}. Therefore these lines are formed in the outermost layers of the envelope which only slightly participate in the pulsation movements. Gillet et al. (1989) assumed a time-average velocity from Ti I and Fe I emissions of about 44 km s^{-1} as a value of the systemic velocity.

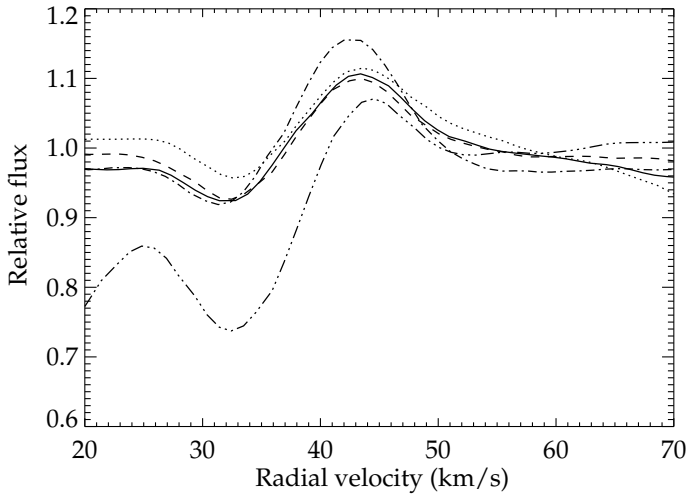

Fig. 8. The Ti I emission lines at 8766.68, 8734.71, 8692.329, 8682.98, 8675.37 Å in the spectrum of R Sct observed on JD = 2454621.6 (the NARVAL database).

4.2. Unstable field of radial velocities

In order to derive the mean radial velocity, V_r, we measured a large number of the pure (without visible emission or splitting) absorptions in the spectra of R Sct, > 400 lines in each spectrum. Taking into account a high probability of differential movements in the extended atmosphere of the star, we looked for the dependence of the radial velocity, measured in different lines, on the excitation potential of their lower level. We have not found such dependence, what permits us to average V_r values measured using the individual metallic lines.

In Table 3 we give V_r values for the selected spectral features and the groups of lines. The second column presents the mean V_r derived from the symmetrical lines, which are variable in time due to star pulsation. When calculating this mean V_r, the lines of Ti I and Fe I with emissions in their red wings were not taken into account. The next columns of Table 3 contain the interstellar component (column 3) and the two stellar components of the Na I D-lines (columns 4 and 5).

Table 3. Heliocentric velocities (in km s^{-1}) of the Na I D-line components in the spectrum of R Sct.

Date [JD]	Stellar velocity	IS		Components 2 and 3			
		D_2	D_1	D_2	D_1	D_2	D_1
2454621.6	37.1	–14.9	–14.7	32.4	32.5	55.8	55.4
2455408.5	45.3	–14.5	–14.3	34.3	33.5	52.7	51.3
2455464.3	29.4	–15.1	–14.5	33.7	33.8	50.6	50.1

All particular features of the velocity field for the observing moment JD = 2455464.3 are shown in the upper panel of Figure 9. For a comparison, similar data from the spectrum on JD = 2455408.5 without Ti I and Fe I emissions and the split of the strongest absorptions are presented in the lower panel of this figure. The center-of-mass velocity of the star is indicated by the horizontal dashed line in the

upper panel. It should be noted that this value, $V_{\rm sys} = 43.8\,{\rm km\,s^{-1}}$ (Preston 1962), is in a good agreement with the value $V_{\rm sys} = 43\,{\rm km\,s^{-1}}$ obtained by Mozurkewich et al. (1987) from atomic emission lines in the near infrared spectrum of R Sct.

In the JD = 2455464.3 spectrum, Na I D-lines have a complex structure and contain three components with the absorption cores corresponding to $V_{\rm r}$ about -14, $+30$ and $+50\,{\rm km\,s^{-1}}$. The first component with –14 km/s is of interstellar origin, its value is in agreement with the positions of interstellar lines in this direction of the Galaxy (Münch 1957). Lèbre & Gillet (1991b) analyzed the structure of D-lines in high resolution spectra and concluded that the blueshifted component could be of interstellar origin or be a circumstellar line formed in a recent mass ejection from stellar envelope.

The red most component at $V_{\rm r} \approx +51\,{\rm km\,s^{-1}}$ origins probably in the circumstellar envelope higher than the region of formation of Ti I and Fe I emissions. As follows from Table 3, the position of this component is slightly variable in time. The third component of D-lines at $V_{\rm r} \approx +30\,{\rm km\,s^{-1}}$, most likely is of photospheric origin. But its position is not always consistent with the positions of other metallic lines (Table 3). As is seen in Figures 10, 11 and 12, both components 2 and 3 contain additional variable features in their wings which are unresolved in our spectra. Lèbre & Gillet (1991b) restored these additional variable components using the Gaussian analysis.

The most interesting peculiarity of the spectra is a split of the strongest low excitation absorption lines which are visible in some spectra. For the JD = 2455464.3 spectrum we found nine split Fe I lines whose lower excitation potential is $\chi_{\rm low}$ = 1–2 eV (at 5269.54, 5371.49, 5397.13, 5405.78, 5429.70, 5434.52, 5446.92, 5455.61 and 6136.62 Å). The blue-shifted components are slightly stronger (by $\sim 8\%$) than the redshifted ones. As follows from the radial velocity picture presented in Figure 9 (upper panel), at this moment of observations both infalling and expanding layers in the extended atmosphere of the star were present.

A diffuse interstellar band (DIB) at 5780 Å was found in the both SAO spectra. The velocities were close to the systemic one. Therefore these bands probably are formed in outer layers of the circumstellar envelope.

5. LUMINOSITY

Parallax of R Sct has been measured by Hipparcos: $\pi = 2.32 \pm 0.82$ mas ($d = 431$ pc). If we assume $E_{B-V} = 0.1$ (see below), this parallax gives $M_V = -3.1^{+0.7}_{-0.9}$ and with $BC = -0.5$ (Ruyter et al. 2005) we obtain $M_{\rm bol} = -3.6^{+0.7}_{-0.9}$ and $\log L/L_\odot = 3.34^{+0.36}_{-0.28}$. However, if the Cepheid period-luminosity relation (see Ruyter et al. 2005) is applied, the distance and luminosity become much larger: $d = 750 \pm 290$ pc and $\log L/L_\odot = 3.97^{+0.25}_{-0.61}$.

We have determined the following equivalent widths of the O I triplet at 7771.9, 7774.2 and 7775.4 Å: 0.15, 0.14 and 0.12 Å. According to the calibration by Arellano Ferro et al. (2003) this gives $M_V \approx -2.0$ mag. With $BC = -0.52$ (Ruyter et al. 2005), we get $M_{\rm bol} \approx -2.5$ mag and $L = 800 L_\odot$. If again the reddening E_{B-V} = 0.1 is assumed, this luminosity corresponds to a distance of ~ 300 pc only, and this supports the lower luminosity determined with the Hipparcos parallax.

The reddening of R Sct is known with a low accuracy. Various estimates of E_{B-V} span from 0.0 (Ruyter et al. 2005) to 0.43 mag (Cardelli 1985). The estimate by Goldsmith et al. (1987) is 0.2 mag, and our estimate from the equivalent

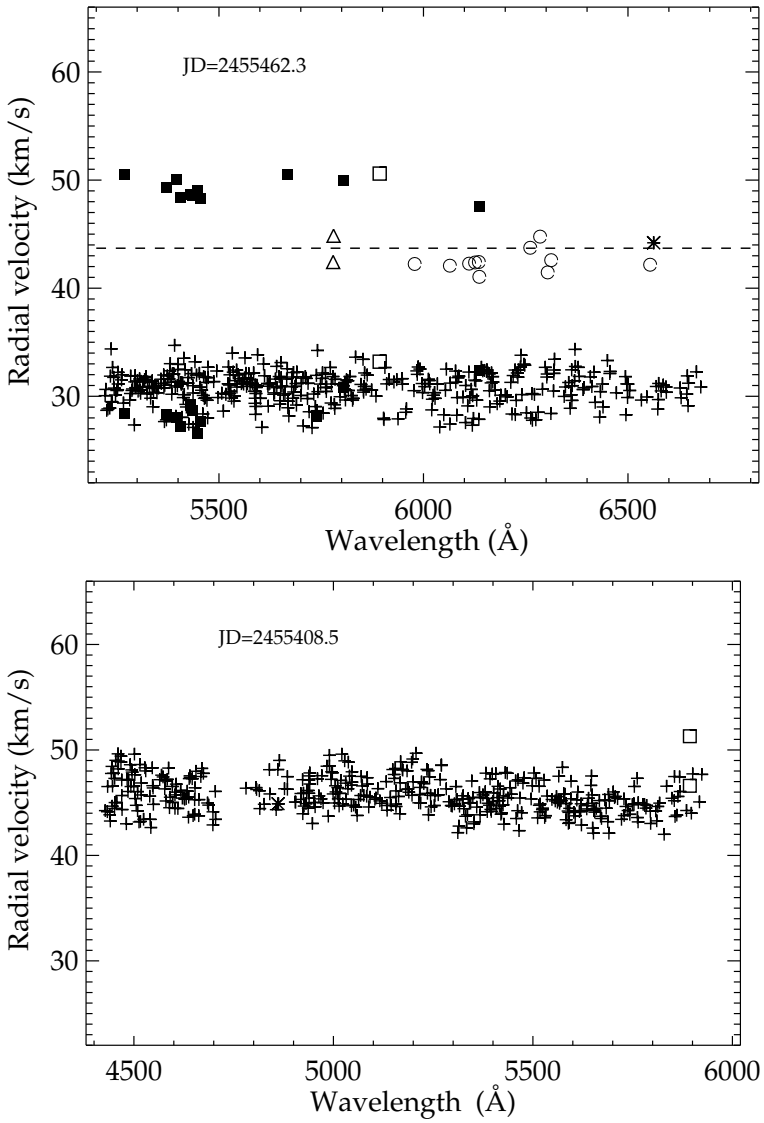

Fig. 9. Radial velocities measured in the SAO spectra of R Sct on two different dates. Crosses correspond to symmetrical absorptions, star symbols – to H I lines, dark squares – to the red and blue components of the spit metallic absorptions, open squares – to the photospheric components of D-lines, open circles – to Fe I emissions, and open triangles – to DIBs. The broken horizontal line corresponds to the velocity of the star's center-of-mass.

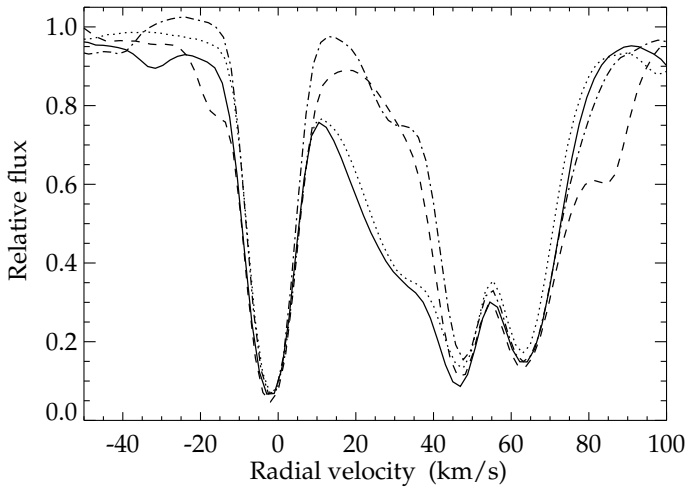

Fig. 10. The Na I D-lines in R Sct SAO spectra on two different dates: JD = 2455464.3: D_2 – solid line and D_1 – dotted line; JD = 2455408.5: D_2 – dashed line and D_1 – dash-dotted line. A good fit of interstellar lines on the two dates is accidental. In this figure the lines are plotted as observed, the velocities are not corrected for the solar motion.

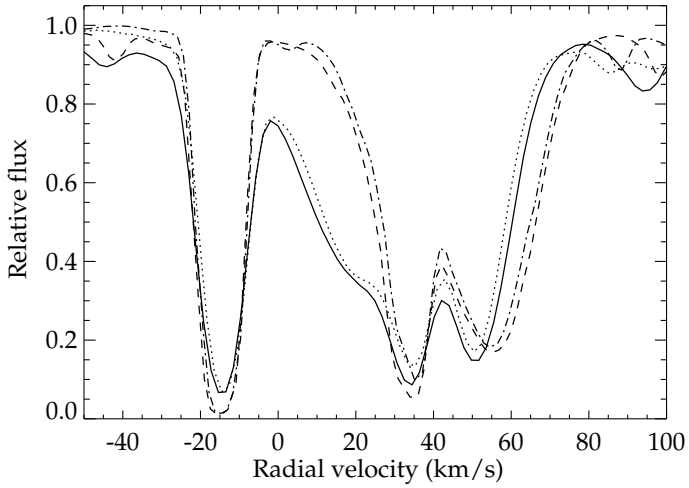

Fig. 11. The Na I D-lines in R Sct SAO spectrum on JD = 2455464.3: D_2 – solid line, D_1 – dotted line. Dashed and dash-dotted lines are for the NARVAL spectrum on JD = 2454621.6. Differently from Figure 10, in this figure the solar velocity is taken into account.

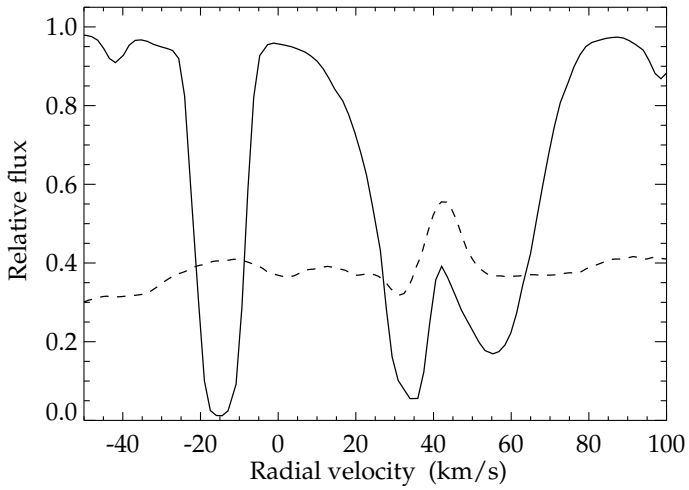

Fig. 12. The Na I D_2-line in the NARVAL spectrum of R Sct on JD = 2454621.6 together with Ti I emission line at 8682.082 Å, with the intensity shift by –0.6.

width of the blue-most Na I D_2 component is ~ 0.3 mag, if that line is interstellar. From the interstellar K I resonance lines we estimated $E_{B-V} = 0.4$. These estimates use the calibration from Munari & Zwitter (1997). The reddening $E_{B-V} = 0.3$ combined with the Hipparcos parallax gives the luminosity $\log L/L_\odot = 3.6$.

The luminosity derived from the parallax corresponds to a tip of RGB or slightly above it. This again shows that R Sct could evolve off the AGB when it had not yet experienced the third dredge-up in thermal pulses, or it have not left the AGB yet.

6. CONCLUSIONS

After the initial assumption that RV Tau stars are the low-mass post-AGB objects which left the AGB quite recently (Jura 1986; Gingold 1974; Eggen 1986), several authors have expressed doubts of such evolutionary status of some individual RV Tau stars, R Sct among them. Zsoldos (1995) and Matsuura et al. (2002) studied R Sct period changes retrospectively to 1800s. As post-AGB objects, RV Tau-type stars are expected to evolve towards higher temperatures at constant luminosities. During such evolution, secular changes in the pulsation period are expected. In the case of R Sct no such period changes have been found. Therefore they concluded that R Sct does not moves towards higher temperatures and has not yet left the AGB. The values of the effective temperature and the period of R Sct are close to those of AGB-stars (Blöcker 1995).

We confirmed the low abundance of heavy elements in the atmosphere of R Sct. We also found that the luminosity of R Sct is rather low at $\log L/L_\odot < 3.7$. The most probable explanation of such chemical composition is that due to its low mass R Sct has not yet experienced the third dredge-up during helium flashes. In that case the initial mass of the star should be less than $1\,M_\odot$ (Wood & Zarro 1981).

ACKNOWLEDGMENTS. This research was supported by the targeted financing project SF00600399S08 of the Estonian Ministry of Education and Research and by the Russian Foundation for Basic Research (project No. 11-02-00319a).

REFERENCES

Arellano Ferro A., Giridhar S., Rojo Arellano E. 2003, RMxAA, 39, 3
Asplund M., Grevesse N., Sauval A. J., Scott P. 2009, ARA&A, 47, 481
Blöcker T. 1995, A&A, 299, 755
Cardelli J. A. 1985, AJ, 90, 1494
Cenarro A. J., Peletier R. F., Sáncez-Blázques P. et al. 2007, MNRAS, 374, 664
Den Hartog E. A., Lawler J. E., Sneden C., Cowan J. J. 2003, ApJS, 148, 543
Eggen O. J. 1986, AJ, 91, 890
Fokin A. B. 1994, A&A, 292, 133
Gillet D., Duquennoy A., Boichet P., Gouiffes C. 1989, A&A, 215, 316
Gingold R. A. 1974, ApJ, 193, 177
Giridhar S., Rao N. K., Lambert D. L. 1994, ApJ, 437, 476
Giridhar S., Lambert D. L., Gonzalez G. 2000, ApJ, 531, 521
Goldsmith M. J., Evans A., Albinson J. S., Bode M. F. 1987, MNRAS, 227, 143
Grevesse N., Noels A., Sauval A. J. 1996, ASP Conf. Ser, 66, 1966
Howell S. B., Bopp B. W., Noah P. V. 1983, PASP, 95, 762
Jura M. 1986, ApJ, 309, 732
Kipper T., Klochkova V. G. 2005, Baltic Astronomy, 14, 215
Lawler J. E., Bonvallet G., Sneden C. 2001, ApJ, 556, 452
Lèbre A., Gillet D. 1991a, A&A, 246, 490
Lèbre A., Gillet D. 1991b, A&A, 251, 549
Lobel A. 2010, http://spectra.freeshell.org
Lodders K. 2003, ApJ, 591, 1220
Luck R. E. 1981, PASP, 93, 211
Luck R. E., Bond H. E. 1989, ApJ, 342, 476
Matsuura M., Yamamaura I., Zijlstra A. A., Bedding T. R. 2002, A&A, 387, 1022
Moore C. E., Minnaert M. G. J., Houtgast J. 1966, *The Solar Spectrum 2935 A to 8770 A*, NBS Mono., 61, Washington
Mozurkewich D., Gehrz R. D., Hinkle K. H., Lambert D. L. 1987, ApJ, 314, 242
Munari U., Zwitter T. 1997, A&A, 318, 269
Münch G. 1957, ApJ, 125, 42
Panchuk V. E., Klochkova V. G., Yushkin M. V., Najdenov I. D. 2009, Journal of Optical Technology, 76, 87
Pollard K. R., Cottrell P. L., Lawson W. A. et al. 1997, MNRAS, 286, 1
Preston G. W. 1962, ApJ, 136, 866
Preston G. W., Krzeminski W., Smak J., Williams J. A. 1963, ApJ, 137, 401
Prugniel P., Vauglin I., Koleva M. 2011, A&A, 531, 165
Rao K., Reddy E. B. 2005, MNRAS, 357, 235
Ralchenko Yu., Kramida A. E., Reader J. & NIST ASD Team, 2011, *NIST Atomic Spectra Database*, http://physics.nist.gov/asd
Ruyter S., van Winckel H., Dominik C. et al. 2005, A&A, 435, 161
Thevenin F. 1989, A&AS, 77, 137
Thevenin F. 1990, A&AS, 82, 179

Van Leeuwen F. 2007, A&A, 474, 653
Wallerstein G., Cox A. N. 1984, PASP, 96, 677
Wiese W. L., Fuhr J. R., Deters T. M. 1996, J. Chem. Ref. Data, Mono. 7
Wing R. F. 1987, JAVSO, 15, 212
Wood P. R., Zarro D. M. 1981, ApJ, 247, 247
Zsoldos E. 1995, A&A, 296, 122

Table 4. Atomic data (wavelengths [Å], lower level excitation potentials ϵ_i [eV], oscillator strengths $\log gf$), equivalent widths [pm] and abundances calculated with the model parameters $T_{\rm eff} = 4500$ K, $\log g = 0.0$ and $\xi_{\rm t} = 4.0\,{\rm km\,s^{-1}}$ for R Sct.

El.	λ	ϵ_i	$\log gf$	EW	$\log\varepsilon$	El.	λ	ϵ_i	$\log gf$	EW	$\log\varepsilon$
C I	4770.000	7.48	−2.44	4.3	8.92	Sc II	5239.820	1.46	−0.77	10.6	1.46
C I	4932.070	7.68	−1.66	7.6	8.91	Sc II	5526.820	1.77	0.02	12.0	1.14
C I	4817.370	7.48	−3.04	2.0	8.99	Sc II	5640.990	1.50	−1.13	6.5	1.44
C I	6014.850	8.64	−1.59	1.0	8.40	Sc II	5657.880	1.51	−0.60	13.5	1.55
						Sc II	5669.040	1.50	−1.20	6.6	1.52
O I	6300.310	0.00	−9.82	17.3	8.73	Sc II	6245.620	1.51	−1.03	6.3	1.29
O I	6363.790	0.00	0.30	9.4	8.63						
						Sc I	5671.830	1.45	0.50	1.3	1.70
Na I	5682.650	2.10	−0.70	16.7	5.87	Sc I	6210.670	0.00	−1.53	4.0	2.22
Na I	6160.750	2.10	−1.26	8.4	5.71						
Na I	6154.229	2.10	−1.56	5.6	5.74	Ti I	4503.760	2.13	−0.80	3.0	4.47
						Ti I	4527.330	0.81	−0.47	19.0	3.90
Mg I	4703.000	4.35	−0.44	33.0	7.47	Ti I	4534.780	0.84	0.28	27.0	4.10
Mg I	5528.420	4.35	−0.50	35.0	7.37	Ti I	4562.640	0.02	−2.66	14.8	4.55
Mg I	5711.100	4.35	−1.72	23.0	7.44	Ti I	4623.100	1.74	0.11	11.1	3.88
Mg I	6319.240	5.11	−2.80	4.9	7.82	Ti I	4639.370	1.73	−0.19	11.1	4.14
						Ti I	4645.190	1.73	−0.56	7.5	4.21
Si I	5665.561	4.92	−2.04	9.0	7.22	Ti I	4693.670	0.02	−2.71	16.0	4.63
Si I	5690.430	4.93	−1.83	10.5	7.14	Ti I	4722.620	1.05	−1.33	10.0	4.27
Si I	5772.150	5.08	−1.75	12.7	7.45	Ti I	4734.670	2.24	−0.86	4.4	4.84
Si I	5793.080	4.93	−2.02	10.0	7.28	Ti I	4742.800	2.24	0.21	9.2	4.23
Si I	5948.550	5.08	−1.23	19.1	7.47	Ti I	4759.280	2.26	0.51	7.3	3.78
Si I	6091.920	5.87	−1.40	5.0	7.29	Ti I	4820.410	1.50	−0.44	14.0	4.28
Si I	6142.490	5.62	−1.48	6.3	7.22	Ti I	4840.880	0.90	−0.51	18.9	3.95
Si I	6145.020	5.61	−1.37	7.0	7.16	Ti I	4870.140	2.25	−0.52	8.3	4.88
Si I	6155.130	5.62	−0.76	13.3	7.15	Ti I	4921.780	2.18	−0.07	8.8	4.38
						Ti I	4926.150	0.82	−2.17	6.6	4.47
Ca I	4578.560	2.52	−0.56	14.1	5.38	Ti I	4928.320	2.15	0.05	6.9	4.04
Ca I	5512.990	2.93	−0.30	9.1	5.02	Ti I	4997.100	0.09	−2.12	21.9	4.54
Ca I	5581.980	2.52	−0.71	14.6	5.37	Ti I	5000.990	2.00	−0.03	10.0	4.18
Ca I	5588.760	2.53	0.21	23.7	5.32	Ti I	5025.570	2.04	0.25	14.3	4.29
Ca I	5590.130	2.52	−0.71	14.7	5.38	Ti I	5039.960	0.02	−1.13	28.0	4.05
Ca I	5601.290	2.53	−0.69	18.0	5.67	Ti I	5043.590	0.84	−1.73	9.5	4.28
Ca I	5857.460	2.93	0.23	21.0	5.48	Ti I	5045.410	0.85	−2.00	7.9	4.44
Ca I	6102.730	1.88	−0.79	23.3	5.24	Ti I	5052.880	2.18	−0.24	8.2	4.46
Ca I	6122.230	1.89	−0.32	31.4	5.47	Ti I	5071.490	1.45	−1.06	9.9	4.46
Ca I	6161.300	2.52	−1.03	9.1	5.18	Ti I	5087.060	1.43	−0.79	10.4	4.20
Ca I	6162.180	1.90	−0.09	33.6	5.43	Ti I	5173.750	0.00	−1.12	28.9	3.95
Ca I	6166.440	2.52	−0.90	8.6	5.00	Ti I	5192.979	0.02	−1.00	28.9	3.95
Ca I	6169.040	2.52	−0.54	13.2	5.01	Ti I	5194.060	2.10	−0.56	4.5	4.31
Ca I	6169.560	2.53	−0.27	17.3	5.10	Ti I	5210.390	0.05	−0.89	30.0	3.95
Ca I	6439.080	2.53	0.47	29.9	5.32	Ti I	5219.710	0.02	−2.29	20.1	4.38
Ca I	6455.610	2.52	−1.36	9.8	5.54	Ti I	5224.311	2.13	0.21	16.0	4.56
Ca I	6471.670	2.53	−0.59	17.6	5.38	Ti I	5295.780	1.07	−1.63	9.0	4.42
Ca I	6493.790	2.52	0.14	23.9	5.15	Ti I	5299.980	1.05	−1.47	4.5	3.82
Ca I	6499.650	2.52	−0.59	14.6	5.13	Ti I	5338.330	0.83	−1.87	5.3	4.00

Table 3. Continued

El.	λ	ϵ_i	$\log gf$	EW	$\log \varepsilon$	El.	λ	ϵ_i	$\log gf$	EW	$\log \varepsilon$
Ti I	5351.070	2.78	0.01	1.6	4.06	V I	5743.430	1.08	−0.97	5.4	3.39
Ti I	5366.640	0.82	−2.58	5.0	4.66	V I	5817.080	1.89	0.09	3.0	3.09
Ti I	5384.640	0.83	−2.91	2.4	4.63	V I	6081.450	1.05	−0.58	9.3	3.24
Ti I	5426.260	0.02	−3.01	13.0	4.55	V I	6090.220	1.08	−0.06	14.1	3.08
Ti I	5460.510	0.05	−2.80	17.0	4.63	V I	6111.650	1.04	−0.72	7.0	3.19
Ti I	5472.710	1.44	−1.57	8.0	4.75	V I	6119.530	1.06	−0.32	11.0	3.11
Ti I	5644.150	2.27	0.21	10.0	4.20	V I	6135.370	1.05	−0.75	7.0	3.23
Ti I	5648.580	2.50	−0.25	2.5	4.15	V I	6150.150	0.30	−1.79	10.0	3.43
Ti I	5716.450	2.30	−0.70	1.5	4.09	V I	6199.190	0.29	−1.28	12.2	3.03
Ti I	5720.450	2.29	−0.90	1.0	4.09	V I	6216.360	0.28	−1.29	9.9	2.89
Ti I	5739.990	2.24	−0.67	2.0	4.12	V I	6224.510	0.29	−2.01	5.4	3.27
Ti I	5774.040	3.01	0.48	3.4	4.21	V I	6233.200	0.28	−2.08	6.3	3.41
Ti I	5866.460	1.07	−0.84	16.5	4.07	V I	6251.830	0.29	−1.34	10.7	3.00
Ti I	5899.300	1.05	−1.15	12.8	4.08	V I	6285.160	0.28	−1.67	8.0	3.12
Ti I	5953.170	1.89	−0.33	10.1	4.21	V I	6292.820	0.29	−1.47	10.0	3.07
Ti I	5965.830	1.88	−0.41	10.0	4.27	V I	6296.490	0.30	−1.59	10.5	3.24
Ti I	5978.550	1.87	−0.50	10.7	4.40						
Ti I	6064.630	1.05	−1.94	6.0	4.36	V II	5303.220	2.28	−1.94	3.0	3.04
Ti I	6098.660	3.06	−0.01	1.7	4.39	V II	5819.930	2.52	−1.70	3.0	3.05
Ti I	6258.110	1.44	−0.36	19.6	4.27						
Ti I	6554.240	1.44	−1.22	8.6	4.32	Cr I	4496.860	0.94	−1.15	27.0	4.90
Ti I	6556.080	1.46	−1.08	13.4	4.56	Cr I	4545.960	0.94	−1.38	22.5	4.54
						Cr I	4569.520	3.12	−0.64	6.0	5.12
Ti II	4468.500	1.13	−0.60	32.0	3.85	Cr I	4591.400	0.97	−1.76	22.2	4.91
Ti II	4493.530	1.08	−2.83	18.8	4.42	Cr I	4616.130	0.98	−1.18	24.8	4.63
Ti II	4500.350	1.08	−3.34	16.0	4.63	Cr I	4626.180	0.97	−1.32	27.0	5.01
Ti II	4501.280	1.12	−0.77	33.0	4.07	Cr I	4646.170	1.03	−0.71	34.0	5.33
Ti II	4568.330	1.22	−3.03	16.9	4.57	Cr I	4646.780	3.10	−0.90	5.6	5.29
Ti II	4589.950	1.24	−1.62	25.8	4.22	Cr I	4651.290	0.98	−1.46	24.3	4.82
Ti II	4609.270	1.18	−3.43	12.0	4.40	Cr I	4652.170	1.00	−1.03	27.6	4.82
Ti II	4636.320	1.17	−3.23	10.9	4.08	Cr I	4664.790	3.13	−0.48	8.5	5.20
Ti II	4764.530	1.24	−2.77	18.0	4.38	Cr I	4697.060	2.71	−1.06	5.3	4.93
Ti II	4865.620	1.12	−2.81	16.6	4.10	Cr I	4708.020	3.17	0.11	6.9	4.49
Ti II	4981.360	1.57	−3.20	5.0	3.88	Cr I	4718.420	3.20	0.10	11.5	4.96
Ti II	5185.910	1.89	−1.37	22.7	4.20	Cr I	4836.860	3.10	−1.14	3.4	5.23
Ti II	5336.790	1.58	−1.63	24.7	4.21	Cr I	4936.340	3.11	−0.34	5.4	4.69
Ti II	5418.780	1.58	−2.11	17.7	3.95	Cr I	4942.480	0.94	−2.29	20.3	5.05
						Cr I	5067.750	2.71	−1.11	5.0	4.89
V I	4577.180	0.00	−1.05	16.2	2.96	Cr I	5091.890	1.00	−3.04	6.4	4.73
V I	4827.460	0.04	−1.48	17.0	3.45	Cr I	5221.760	3.38	−0.87	3.5	5.28
V I	4851.500	0.00	−1.14	22.7	3.56	Cr I	5296.700	0.98	−1.41	31.0	5.12
V I	5240.880	2.37	0.33	2.3	3.39	Cr I	5297.390	2.90	0.17	18.0	4.98
V I	5668.370	1.08	−1.03	6.0	3.52	Cr I	5345.810	1.00	−0.98	30.0	4.63
V I	5670.860	1.08	−0.42	13.5	3.46	Cr I	5345.810	1.00	−0.98	30.0	4.63
V I	5703.590	1.05	−0.21	14.2	3.26	Cr I	5712.780	3.01	−1.30	3.1	5.13
V I	5727.060	1.08	−0.01	15.7	3.20	Cr I	5783.070	3.32	−0.50	2.4	4.58
V I	5727.660	1.05	−0.87	7.8	3.46	Cr I	5787.930	3.32	−0.08	5.8	4.63
V I	5731.220	1.06	−0.73	9.6	3.47	Cr I	6661.080	4.19	−0.19	1.3	4.99
V I	5737.070	1.06	−0.74	7.5	3.32						

Table 3. Continued

El.	λ	ϵ_i	$\log gf$	EW	$\log \varepsilon$	El.	λ	ϵ_i	$\log gf$	EW	$\log \varepsilon$
Cr II	4554.990	4.07	−1.28	14.2	5.18	Fe I	5223.189	3.63	−1.78	6.6	6.29
Cr II	4558.650	4.07	−0.45	21.0	5.20	Fe I	5228.380	4.22	−1.29	14.0	7.20
Cr II	4616.630	4.07	−1.36	12.5	5.05	Fe I	5231.400	3.57	−3.04	3.4	7.10
Cr II	4824.140	3.87	−0.97	19.7	5.20	Fe I	5236.210	4.19	−1.50	7.7	6.81
Cr II	5237.320	4.07	−1.16	15.0	5.02	Fe I	5242.500	3.63	−0.97	21.8	6.86
Cr II	5305.870	3.83	−2.36	9.0	5.29	Fe I	5243.780	4.26	−1.15	13.7	7.08
Cr II	5308.430	4.07	−1.85	8.0	4.93	Fe I	5249.110	4.47	−1.48	9.1	7.26
Cr II	5313.590	4.07	−1.65	11.2	5.09	Fe I	5250.220	0.12	−4.94	34.4	7.26
Cr II	5334.870	4.07	−1.56	11.0	4.98	Fe I	5253.470	3.28	−1.57	21.0	6.92
						Fe I	5267.270	4.37	−1.60	4.5	6.79
Mn I	4739.110	2.94	−0.49	syn	4.80	Fe I	5285.130	4.43	−1.64	5.5	7.03
Mn I	4761.530	2.95	−0.14	syn	4.58	Fe I	5288.530	3.69	−1.51	15.6	6.88
Mn I	4765.860	2.94	−0.08	syn	4.65	Fe I	5293.960	4.14	−1.87	7.0	7.05
Mn I	4823.510	2.32	0.14	syn	4.15	Fe I	5294.550	3.64	−2.86	4.0	7.08
Mn I	5377.610	3.84	−0.11	syn	4.85	Fe I	5295.320	4.41	−1.69	5.4	7.04
Mn I	5394.680	0.00	−3.50	syn	4.55	Fe I	5302.310	3.28	−0.72	30.0	6.99
Mn I	5407.420	2.14	−1.74	syn	5.03	Fe I	5307.370	1.61	−2.99	34.0	7.37
Mn I	5420.350	2.14	−1.46	syn	5.10	Fe I	5315.080	4.37	−1.55	7.0	7.01
Mn I	5432.550	0.00	−3.80	syn	4.80	Fe I	5321.110	4.43	−0.95	7.0	6.48
Mn I	5457.470	2.16	−2.61	syn	5.35	Fe I	5322.050	2.28	−2.80	24.1	7.06
Mn I	5470.640	2.16	−1.70	syn	5.07	Fe I	5324.190	3.21	−0.10	36.6	6.94
Mn I	5505.890	2.18	−2.23	syn	4.81	Fe I	5326.820	4.41	−2.10	1.8	6.87
Mn I	5516.770	2.18	−1.85	syn	5.20	Fe I	5330.000	4.07	−1.19	15.0	6.99
Mn I	5537.760	2.19	−2.02	syn	5.25	Fe I	5333.770	3.02	−3.58	4.5	7.08
Mn I	6013.500	3.07	−0.25	syn	4.80	Fe I	5339.940	3.26	−0.65	34.0	7.30
						Fe I	5358.120	3.30	−3.51	3.8	7.28
Mn I	6016.650	3.07	−0.22	17.2	4.92	Fe I	5361.630	4.41	−1.43	10.0	7.21
Mn I	6021.800	3.08	0.04	19.6	4.92	Fe I	5364.880	4.44	0.23	27.0	7.24
						Fe I	5365.410	3.57	−1.02	18.0	6.44
Fe I	5031.920	4.37	−1.67	4.8	6.93	Fe I	5367.480	4.41	0.44	26.0	6.89
Fe I	5044.220	2.85	−2.04	20.1	6.78	Fe I	5373.710	4.47	−0.86	13.0	6.96
Fe I	5049.830	2.28	−1.36	37.5	7.19	Fe I	5379.580	3.69	−1.51	15.5	6.86
Fe I	5054.650	3.64	−1.92	9.0	6.69	Fe I	5383.380	4.31	0.65	29.0	6.86
Fe I	5058.490	3.64	−2.83	3.2	6.97	Fe I	5385.590	3.69	−2.97	1.0	6.57
Fe I	5067.160	4.22	−0.97	18.5	7.36	Fe I	5386.340	4.15	−1.77	6.0	6.85
Fe I	5074.750	4.22	−0.20	24.3	7.20	Fe I	5387.480	4.14	−2.03	3.1	6.74
Fe I	5088.160	4.15	−1.78	6.8	6.97	Fe I	5391.460	4.15	−0.83	22.0	7.39
Fe I	5090.780	4.26	−0.40	19.9	6.98	Fe I	5393.180	3.24	−0.72	29.0	6.78
Fe I	5104.030	3.02	−2.87	15.8	7.43	Fe I	5398.290	4.44	−0.67	15.3	6.96
Fe I	5121.630	4.28	−0.81	18.4	7.24	Fe I	5401.270	4.32	−1.92	5.4	7.14
Fe I	5125.130	4.22	−0.14	27.5	7.48	Fe I	5410.920	4.47	0.40	30.0	7.42
Fe I	5133.700	4.18	0.14	28.7	7.28	Fe I	5412.790	4.43	−1.72	5.6	7.10
Fe I	5141.750	2.42	−1.96	28.5	6.96	Fe I	5415.210	4.39	0.64	29.0	6.97
Fe I	5143.730	2.20	−3.79	15.7	7.23	Fe I	5429.710	0.96	−1.88	65.5	7.02
Fe I	5162.280	4.18	0.02	24.8	6.95	Fe I	5434.530	1.01	−2.12	56.5	7.12
Fe I	5177.240	3.69	−2.42	8.3	7.17	Fe I	5436.600	2.28	−2.96	24.0	7.16
Fe I	5180.070	4.47	−1.26	9.9	7.12	Fe I	5441.350	4.31	−1.73	6.4	7.05
Fe I	5187.920	4.14	−1.37	15.1	7.29	Fe I	5445.050	4.39	−0.02	23.0	6.98
Fe I	5198.720	2.22	−2.14	32.0	7.22	Fe I	5452.100	3.64	−2.86	4.5	7.13
Fe I	5215.190	3.26	−0.87	28.4	6.98	Fe I	5456.530	3.60	−3.21	3.3	7.27
Fe I	5217.400	3.21	−1.07	25.7	6.81	Fe I	5461.560	4.44	−1.90	6.0	7.33

Table 3. Continued

El.	λ	ϵ_i	$\log gf$	EW	$\log \varepsilon$	El.	λ	ϵ_i	$\log gf$	EW	$\log \varepsilon$
Fe I	5464.290	4.14	−1.40	7.0	6.56	Fe I	5760.360	3.64	−2.49	6.1	6.90
Fe I	5466.400	4.37	−0.63	17.0	6.97	Fe I	5762.420	3.64	−2.28	9.5	6.99
Fe I	5470.090	4.44	−1.81	4.8	7.11	Fe I	5763.000	4.21	−0.45	22.0	6.99
Fe I	5473.910	4.15	−0.76	17.7	6.88	Fe I	5775.090	4.22	−1.30	12.8	7.03
Fe I	5491.840	4.19	−2.19	2.5	6.84	Fe I	5793.920	4.22	−1.70	8.0	7.01
Fe I	5494.470	4.07	−2.09	5.9	7.05	Fe I	5805.771	5.03	−1.59	3.5	7.42
Fe I	5522.450	4.21	−1.55	9.5	7.01	Fe I	5806.729	4.61	−1.05	9.5	6.98
Fe I	5525.550	4.23	−1.09	11.4	6.73	Fe I	5807.790	3.29	−3.41	3.5	7.07
Fe I	5536.600	2.83	−3.81	4.2	7.01	Fe I	5809.220	3.88	−1.84	11.0	6.97
Fe I	5539.290	3.64	−2.66	5.0	6.99	Fe I	5811.920	4.14	−2.43	2.6	7.01
Fe I	5543.200	3.69	−1.57	13.0	6.63	Fe I	5814.810	4.28	−1.97	4.6	7.02
Fe I	5543.940	4.22	−1.14	13.0	6.90	Fe I	5816.380	4.55	−0.60	14.0	6.83
Fe I	5546.510	4.37	−1.31	11.1	7.10	Fe I	5827.880	3.28	−3.41	4.0	7.12
Fe I	5547.000	4.22	−1.91	7.0	7.16	Fe I	5838.380	3.94	−2.34	7.2	7.22
Fe I	5557.990	4.47	−1.28	10.0	7.10	Fe I	5849.690	3.69	−2.99	2.9	7.06
Fe I	5560.220	4.43	−1.19	10.0	6.96	Fe I	5852.230	4.55	−1.33	8.0	7.06
Fe I	5565.710	4.61	−0.29	20.0	7.19	Fe I	5853.160	1.48	−5.28	11.3	7.29
Fe I	5567.400	2.61	−2.56	20.0	6.83	Fe I	5855.090	4.61	−1.48	3.5	6.79
Fe I	5569.630	3.42	−0.49	31.3	6.96	Fe I	5856.100	4.29	−1.33	5.8	6.53
Fe I	5572.850	3.40	−0.28	37.0	7.29	Fe I	5859.600	4.55	−0.40	14.0	6.63
Fe I	5576.100	3.43	−1.00	27.0	7.03	Fe I	5861.110	4.28	−2.45	1.2	6.82
Fe I	5579.350	4.23	−2.40	3.1	7.20	Fe I	5862.370	4.55	−0.06	17.2	6.57
Fe I	5586.770	3.37	−0.12	35.0	6.89	Fe I	5873.220	4.26	−2.14	4.8	7.18
Fe I	5607.670	4.15	−2.27	3.8	7.07	Fe I	5881.280	4.61	−1.84	4.5	7.27
Fe I	5611.370	3.63	−2.99	4.0	7.17	Fe I	5883.810	3.96	−1.36	15.0	6.91
Fe I	5618.640	4.21	−1.28	10.9	6.84	Fe I	5902.480	4.59	−1.81	4.2	7.18
Fe I	5619.610	4.39	−1.70	7.1	7.16	Fe I	5905.680	4.65	−0.73	10.0	6.74
Fe I	5633.950	4.99	−0.27	12.0	6.91	Fe I	5916.260	2.45	−2.99	21.0	7.04
Fe I	5635.830	4.26	−1.89	5.3	7.02	Fe I	5929.680	4.55	−1.41	7.8	7.11
Fe I	5638.271	4.22	−0.87	15.0	6.81	Fe I	5930.190	4.65	−0.23	16.6	6.82
Fe I	5641.450	4.26	−1.18	13.0	6.98	Fe I	5934.660	3.93	−1.17	18.5	6.99
Fe I	5650.689	5.08	−0.96	7.0	7.26	Fe I	5956.710	0.86	−4.61	30.9	7.24
Fe I	5651.480	4.47	−2.00	3.0	7.07	Fe I	5958.340	2.18	−4.49	10.5	7.36
Fe I	5652.330	4.26	−1.95	5.0	7.04	Fe I	5976.790	3.94	−1.31	16.2	6.94
Fe I	5653.870	4.39	−1.64	6.5	7.05	Fe I	5984.830	4.73	−0.34	18.8	7.21
Fe I	5661.350	4.28	−1.74	5.5	6.90	Fe I	5987.070	4.79	−0.56	12.2	6.92
Fe I	5679.030	4.65	−0.92	10.0	6.95	Fe I	6003.020	3.88	−1.12	19.6	6.96
Fe I	5686.540	4.55	−0.45	18.0	7.06	Fe I	6007.970	4.65	−0.97	12.7	7.21
Fe I	5701.560	2.56	−2.22	25.0	6.83	Fe I	6008.570	3.88	−1.08	20.9	7.03
Fe I	5705.470	4.30	−1.36	7.2	6.72	Fe I	6020.190	4.61	−0.27	23.2	7.39
Fe I	5706.010	4.61	−0.53	16.0	7.04	Fe I	6024.070	4.55	−0.12	21.8	7.03
Fe I	5717.840	4.28	−1.13	13.0	6.94	Fe I	6056.010	4.73	−0.46	12.8	6.79
Fe I	5720.900	4.55	−1.95	3.3	7.16	Fe I	6065.490	2.61	−1.53	31.3	6.63
Fe I	5724.470	4.28	−2.64	1.5	7.13	Fe I	6079.020	4.65	−1.12	8.5	6.99
Fe I	5731.770	4.26	−1.30	12.2	7.04	Fe I	6082.720	2.22	−3.57	21.6	7.32
Fe I	5732.300	4.99	−1.56	3.5	7.33	Fe I	6093.650	4.61	−1.50	4.6	6.93
Fe I	5738.240	4.22	−2.34	3.0	7.09	Fe I	6096.670	3.98	−1.93	7.9	6.91
Fe I	5741.860	4.26	−1.85	6.3	7.07	Fe I	6097.100	2.18	−4.84	3.2	7.00
Fe I	5752.040	4.55	−1.27	11.1	7.26	Fe I	6098.250	4.56	−1.89	2.5	6.95
Fe I	5753.130	4.26	−0.69	17.0	6.84	Fe I	6102.180	4.83	−0.63	15.6	7.34

Table 3. Continued

El.	λ	ϵ_i	$\log gf$	EW	$\log \varepsilon$	El.	λ	ϵ_i	$\log gf$	EW	$\log \varepsilon$
Fe I	6103.189	4.83	−0.77	15.3	7.46	Fe I	6613.830	1.01	−5.79	10.9	7.05
Fe I	6137.700	2.59	−1.40	37.0	7.02	Fe I	6625.040	1.01	−5.34	19.1	7.10
Fe I	6151.620	2.18	−3.30	22.6	7.05	Fe I	6627.560	4.55	−1.68	4.6	7.01
Fe I	6157.730	4.07	−1.26	15.5	6.98	Fe I	6646.970	2.61	−3.99	7.1	7.10
Fe I	6187.410	2.83	−4.34	3.5	7.39	Fe I	6648.120	1.01	−5.28	13.3	6.69
Fe I	6187.990	3.94	−1.72	9.8	6.79	Fe I	6663.450	2.42	−2.48	32.0	7.21
Fe I	6200.320	2.61	−2.44	23.5	6.86	Fe I	6678.000	2.69	−1.42	35.1	6.80
Fe I	6213.440	2.22	−2.48	29.0	6.81						
Fe I	6219.290	2.20	−2.43	31.8	6.98	Fe II	4576.340	2.84	−2.92	25.0	7.45
Fe I	6226.740	3.88	−2.22	5.5	6.83	Fe II	4620.520	2.83	−3.24	23.0	7.49
Fe I	6232.650	3.65	−1.22	18.6	6.63	Fe II	4713.180	2.78	−4.65	8.1	7.08
Fe I	6240.650	2.22	−3.23	19.7	6.80	Fe II	4893.820	2.83	−4.45	14.0	7.54
Fe I	6246.330	3.60	−0.73	24.0	6.53	Fe II	4923.930	2.89	−1.32	38.1	6.99
Fe I	6252.560	2.40	−1.69	34.0	6.71	Fe II	5132.670	2.81	−3.98	15.0	7.10
Fe I	6265.140	2.18	−2.55	29.5	6.85	Fe II	5161.180	2.85	−4.48	6.8	6.79
Fe I	6270.230	2.86	−2.46	18.8	6.83	Fe II	5256.930	2.89	−4.25	13.0	7.25
Fe I	6271.280	3.33	−2.70	5.9	6.66	Fe II	5325.561	3.22	−3.12	22.3	7.52
Fe I	6290.970	4.73	−0.97	13.0	7.29	Fe II	5337.730	3.23	−3.89	14.0	7.41
Fe I	6297.800	2.22	−2.74	28.7	7.02	Fe II	5362.870	3.20	−2.74	26.0	7.52
Fe I	6301.510	3.65	−0.72	25.2	6.63	Fe II	5414.080	3.22	−3.54	12.1	6.84
Fe I	6311.500	2.83	−3.14	12.4	6.97	Fe II	5425.260	3.20	−3.16	19.0	7.13
Fe I	6315.810	4.07	−1.71	9.1	6.88	Fe II	5525.140	3.27	−3.95	10.0	7.08
Fe I	6318.030	2.45	−2.34	30.8	7.11	Fe II	5534.850	3.24	−2.73	21.0	6.96
Fe I	6335.340	2.20	−2.18	32.6	6.76	Fe II	5545.280	2.58	−5.91	2.9	7.35
Fe I	6344.150	2.43	−2.92	22.1	6.95	Fe II	5725.950	3.42	−4.83	2.4	7.13
Fe I	6353.850	0.91	−6.48	5.7	7.23	Fe II	5732.730	3.39	−4.67	4.0	7.23
Fe I	6355.040	2.84	−2.35	25.5	7.21	Fe II	5991.380	3.15	−3.54	16.3	7.09
Fe I	6380.750	4.19	−1.38	9.9	6.76	Fe II	6084.100	3.20	−3.78	12.0	6.99
Fe I	6392.540	2.28	−4.04	10.4	6.99	Fe II	6113.330	3.22	−4.11	9.0	7.04
Fe I	6393.610	2.43	−1.43	37.9	6.80	Fe II	6129.730	3.20	−4.72	7.5	7.46
Fe I	6408.030	3.69	−1.02	21.9	6.72	Fe II	6149.250	3.89	−2.72	15.0	7.05
Fe I	6411.660	3.65	−0.60	26.7	6.63	Fe II	6238.390	3.89	−2.63	16.0	7.05
Fe I	6421.360	2.28	−2.03	35.3	6.94	Fe II	6369.460	2.89	−4.16	10.6	6.81
Fe I	6430.860	2.18	−2.01	36.5	6.88	Fe II	6416.930	3.89	−2.65	14.0	6.87
Fe I	6436.410	4.19	−2.46	2.4	7.01	Fe II	6432.680	2.89	−3.52	15.0	6.58
Fe I	6475.630	2.56	−2.94	22.1	7.10	Fe II	6442.950	5.55	−2.89	2.4	7.57
Fe I	6498.940	0.96	−4.69	30.5	7.23	Fe II	6456.390	3.90	−2.10	22.0	7.10
Fe I	6518.370	2.83	−2.46	22.0	6.99						
Fe I	6533.940	4.56	−1.46	9.3	7.25	Co I	4792.860	3.25	−0.07	8.1	4.15
Fe I	6591.330	4.59	−2.07	2.0	7.02	Co I	4813.480	3.22	0.05	12.7	4.39
Fe I	6591.330	4.59	−2.07	2.0	7.02	Co I	4987.850	0.58	−3.49	13.0	4.41
Fe I	6556.811	4.79	−1.97	2.8	7.34	Co I	5094.950	2.04	−1.99	5.7	4.26
Fe I	6569.220	4.73	−0.42	16.8	7.04	Co I	5149.800	1.74	−2.76	6.5	4.70
Fe I	6574.250	0.99	−5.00	24.8	7.12	Co I	5212.690	3.51	−0.11	7.3	4.38
Fe I	6575.040	2.59	−2.71	24.6	7.09	Co I	5301.050	1.71	−1.99	11.8	4.30
Fe I	6581.220	1.48	−4.68	17.9	7.05	Co I	5342.710	4.02	0.69	8.0	4.28
Fe I	6591.330	4.59	−2.07	2.0	7.02	Co I	5352.050	3.58	0.06	7.4	4.30
Fe I	6592.930	2.73	−1.47	35.8	7.00	Co I	5359.200	4.15	0.34	3.0	4.21
Fe I	6593.880	2.43	−2.42	30.7	7.07	Co I	5369.600	1.74	−1.65	13.8	4.13
Fe I	6597.570	4.79	−1.07	11.6	7.33	Co I	5381.770	4.24	−0.03	1.9	4.46
Fe I	6608.040	2.28	−4.03	9.3	6.88	Co I	5469.280	1.88	−2.53	7.0	4.65
Fe I	6609.120	2.56	−2.69	21.1	6.77	Co I	5483.910	3.63	−0.48	4.0	4.52

Table 3. Continued

El.	λ	ϵ_i	$\log gf$	EW	$\log \varepsilon$	El.	λ	ϵ_i	$\log gf$	EW	$\log \varepsilon$
Co I	5530.790	1.71	−2.06	12.9	4.41	Ni I	5553.710	1.94	−3.24	15.2	5.90
Co I	5647.240	2.28	−1.56	8.3	4.30	Ni I	5578.730	1.68	−2.64	21.0	5.40
Co I	5915.570	2.14	−2.00	6.9	4.40	Ni I	5587.870	1.94	−2.14	26.1	5.67
Co I	5935.400	1.88	−2.68	5.0	4.55	Ni I	5589.370	3.90	−1.14	6.1	5.60
Co I	6117.000	1.79	−2.49	6.7	4.39	Ni I	5592.270	1.95	−2.59	21.1	5.70
Co I	6189.000	1.71	−2.46	11.4	4.61	Ni I	5593.750	3.90	−0.84	8.2	5.48
Co I	6429.900	2.14	−2.43	2.8	4.30	Ni I	5625.330	4.09	−0.70	8.0	5.56
Co I	6455.000	3.63	−0.25	4.8	4.31	Ni I	5643.090	4.17	−1.25	2.0	5.45
Co I	6477.870	3.78	−0.71	2.5	4.62	Ni I	5682.210	4.11	−0.47	9.9	5.50
Co I	6632.470	2.28	−2.00	6.0	4.44	Ni I	5694.990	4.09	−0.61	8.7	5.52
						Ni I	5748.360	1.68	−3.26	16.4	5.64
Ni I	4551.230	4.17	−0.88	2.7	5.35	Ni I	5760.840	4.11	−0.80	6.5	5.53
Ni I	4686.220	3.60	−0.64	12.5	5.40	Ni I	5805.230	4.17	−0.64	6.5	5.44
Ni I	4703.820	3.66	−0.74	11.6	5.49	Ni I	5847.010	1.68	−3.21	13.3	5.34
Ni I	4715.770	3.54	−0.33	18.3	5.56	Ni I	5892.880	1.99	−2.34	24.4	5.70
Ni I	4754.760	3.64	−0.97	11.4	5.67	Ni I	5996.740	4.24	−1.06	2.9	5.50
Ni I	4756.520	3.48	−0.34	18.9	5.54	Ni I	6007.320	1.68	−3.34	12.8	5.42
Ni I	4806.990	3.68	−0.64	16.6	5.85	Ni I	6053.690	4.24	−1.07	4.5	5.73
Ni I	4821.130	4.15	−0.85	6.7	5.77	Ni I	6108.120	1.68	−2.44	23.0	5.21
Ni I	4852.560	3.54	−1.07	10.6	5.56	Ni I	6128.980	1.68	−3.32	14.5	5.50
Ni I	4857.400	3.74	−1.20	10.6	5.94	Ni I	6186.720	4.11	−0.96	4.0	5.38
Ni I	4866.280	3.54	−0.31	18.0	5.47	Ni I	6204.610	4.09	−1.14	5.3	5.69
Ni I	4904.420	3.54	−0.17	20.0	5.51	Ni I	6271.770	3.31	−2.62	2.3	5.77
Ni I	4930.800	3.85	−1.66	4.1	5.90	Ni I	6327.600	1.68	−3.15	17.4	5.49
Ni I	4935.830	3.94	−0.36	11.8	5.43	Ni I	6360.820	4.17	−1.28	4.6	5.84
Ni I	4937.350	3.61	−0.40	19.5	5.75	Ni I	6378.260	4.15	−0.90	10.6	5.98
Ni I	4953.210	3.74	−0.66	16.4	5.90	Ni I	6482.810	1.94	−2.63	18.0	5.36
Ni I	5000.350	3.64	−0.43	19.8	5.84	Ni I	6532.880	1.94	−3.39	14.0	5.83
Ni I	5017.580	3.54	−0.08	22.4	5.61	Ni I	6586.320	1.95	−2.81	16.0	5.39
Ni I	5032.730	3.90	−1.27	3.4	5.47	Ni I	6635.140	4.42	−0.83	4.5	5.67
Ni I	5035.370	3.64	0.29	25.7	5.70	Ni I	6643.640	1.68	−2.30	31.2	5.58
Ni I	5082.350	3.66	−0.54	13.0	5.33						
Ni I	5084.110	3.68	0.03	19.0	5.33	Cu I	5105.550	1.39	−1.50	22.8	3.17
Ni I	5094.420	3.83	−1.08	4.4	5.32	Cu I	5782.140	1.64	−1.78	23.0	3.60
Ni I	5099.940	3.68	−0.10	20.0	5.56						
Ni I	5102.970	1.68	−2.62	21.0	5.51	Zn I	4722.160	4.03	−0.34	18.9	4.15
Ni I	5115.400	3.83	−0.11	17.0	5.48	Zn I	4810.540	4.08	−0.14	19.6	4.06
Ni I	5130.370	3.84	−1.25	6.9	5.76	Zn I	6362.350	5.80	0.15	6.7	4.29
Ni I	5155.130	3.90	−0.66	11.7	5.65						
Ni I	5155.771	3.90	−0.09	18.2	5.64	Y II	4883.690	1.03	0.07	15.0	0.40
Ni I	5157.979	3.61	−1.59	6.0	5.72	Y II	5087.430	1.08	−0.17	5.4	−0.26
Ni I	5176.570	3.90	−0.44	12.9	5.52	Y II	5402.780	1.84	−0.51	2.3	0.49
Ni I	5259.490	3.74	−1.50	2.8	5.37	Y II	5200.410	0.99	−0.60	8.4	0.34
Ni I	5388.350	1.94	−3.55	7.3	5.65						
Ni I	5424.650	1.95	−2.77	15.8	5.51	Ce II	4628.160	0.52	0.22	5.0	−0.32
Ni I	5435.870	1.99	−2.60	18.0	5.58	Ce II	4773.960	0.92	0.27	3.2	−0.15
Ni I	5452.850	3.80	−1.67	2.2	5.48						
Ni I	5510.020	3.85	−0.90	8.0	5.47	Zr I	6143.180	0.07	−1.14	1.8	1.39

Table 3. Continued

El.	λ	ϵ_i	$\log gf$	EW	$\log \varepsilon$	El.	λ	ϵ_i	$\log gf$	EW	$\log \varepsilon$
Zr I	6134.570	0.00	−1.19	1.4	1.22	Nd II	5293.170	0.82	0.10	5.3	−0.15
Zr I	6304.320	0.54	−0.36	2.1	1.36	Nd II	5485.710	1.26	−0.12	1.8	0.03
Zr I	5735.710	0.50	−0.39	0.9	1.00	Nd II	4859.030	0.32	−0.44	7.1	0.01
Zr I	5885.630	0.57	−0.89	0.2	0.92	Nd II	5548.450	0.55	−1.27	1.5	0.21
Zr I	5664.521	0.63	−0.82	0.6	1.44						
Zr I	5277.420	0.54	−0.57	1.0	1.35	Sm II	4642.240	0.38	−0.52	4.4	−0.31
						Sm II	4676.930	0.04	−0.86	2.5	−0.69
Ba II	4934.090	0.00	−0.16	30.3	0.35	Sm II	4467.340	0.66	0.30	4.5	−0.73
Ba II	5853.690	0.60	−0.91	20.6	0.55						
Ba II	6141.729	0.70	−0.03	29.9	0.57	Eu II	6437.700	1.32	−0.27	3.4	−0.22
Nd II	4706.550	0.00	−0.71	6.1	−0.20						
Nd II	4811.350	0.06	−1.02	3.4	−0.17						
Nd II	5092.800	0.38	−0.61	2.0	−0.48						